Original Article

Effect of activation temperature of Yttria Stabilized Zirconia (YSZ)/ZnO nanorods thin film on photoelectrochemical cell performance

Nandang Mufti [a,b,], Eprilia Trikusuma Sari [a], M. Tommy Hasan Abadi [a], Atika Sari Puspita Dewi [a], Markus Diantoro [a,b], Muhammad Safwan Aziz [c], Zulhadjri [d], Henry Setiyanto [e], Sunaryono [a], Poppy Puspitasari [f]*

[a] Department of Physics, Faculty of Mathematics and Natural Sciences, Universitas Negeri Malang, Jl. Semarang 5, Malang, 65145, Indonesia
[b] Center of Advanced Materials for Renewable Energy, Universitas Negeri Malang, Jl. Semarang 5, Malang, 65145, Indonesia
[c] Laser Centre, Ibnu Sina Institute for Scientific and Industrial Research, Universiti Teknologi Malaysia (UTM), 81310, Skudai, Johor D.T., Malaysia
[d] Department of Chemistry, Faculty of Mathematics and Natural Sciences, Universitas Andalas, Kampus Limau Manis Padang 25163, Indonesia
[e] Analytical Chemistry Research Group, Institut Teknologi Bandung, Bandung, 40132, Indonesia
[f] Mechanical Engineering Department, Engineering Faculty, State University of Malang, 5 Semarang Str., 65145, Malang, East Java, Indonesia

ARTICLE INFO

ABSTRACT

A photoelectrochemical cell (PEC) is a device that converts solar energy into electrical energy stored in the form of hydrogen and oxygen. The n-type semiconductor that shows promising potential as a PEC cell device is known as ZnO. ZnO in the form of nanorods (NRs) is considered capable of increasing the conversion efficiency of PEC performance due to the large surface area. However, in the energy conversion process, the photoactive layer of the PEC cell corrode easily in the electrolyte solution, reducing the stability of the current produced and shortening the lifetime of the PEC cell. In this study, the stability improvement using solid electrolytes in photoelectrochemical technology was studied. Yttria Stabilized Zirconia is a type of solid electrolyte that has high mechanical properties and ionic conductivity. Activation of YSZ powder at various temperatures is considered very instrumental to the efficiency of the PEC cell device. XRD, SEM-EDX, and UV–Vis characterized the samples. For efficiency measurement through I–V testing, it is equipped with photodetectors such as photoresponse of current and voltage as well as photostability. The higher the YSZ activation temperature, several results were obtained, the larger ZnO NRs/

---

* Corresponding author.
  E-mail address: nandang.mufti.fmipa@um.ac.id (N. Mufti).

YSZ particle size, the lower the thickness of the film, the higher the absorbance value, and the smaller the band gap. In addition, sample agglomeration occurs at the temperature with the lowest activation and sample response when irradiated enough. Finally, the efficiency of the cell increases, namely at the YSZ activation temperature of 1400 °C, where 1% is produced.

1. Introduction

Along with the development of science, technology, and industry, the need for electrical energy is also increasing. Around 87% of the world's energy consumption comes from fossils (petroleum, natural gas, and coal) which are not renewable and naturally have a negative impact on the environment [1]. Therefore, the use of environmentally friendly sources needs to be considered, one of which is solar energy [2]. Technically, solar energy can be converted into electrical energy through photovoltaic mechanisms using solar cells [3]. In 1972, the first TiO_2-based photoelectrochemical cell (PEC) research was published and produced a current density of 0.5 mA/cm^2 [4]. However, even in the latest research, PEC cells with a tandem structure recorded a current density value of more than 15 mA/cm^2 [5]. The main components of PEC-based solar cell devices consist of photoanodes, counter electrodes, and electrolytes [6]. In contrast, the semiconductor materials that are often used as photoanodes are ZnO, TiO_2, Cu_2O, WO_3 and Fe_2O_3 [7].

ZnO is an n-type semiconductor material that is often used as a photoanode of solar cells because it has an energy band gap of ~3.37 eV [8], high electron mobility up to 5.000 cm^2/Vs [9] and structural stability when nano [10]. Its existence is easy to find in nature, in addition to being non-toxic, environmentally friendly, and economical [11]. ZnO is widely used in various applications such as solar cells [12], gas sensors [13], and supercapacitors [14]. Besides being applied in bulk conditions, ZnO can be utilized in one-dimensional structural nanorods by modifying the crystal structure [15]. ZnO nanorod has the potential to improve light absorption ability compared to other structures [16]. In addition, ZnO nanorods have a large surface area that is 7 times higher than the two-dimensional thin film ZnO structure [17].

Many studies have been conducted on PEC based on the ZnO nanorod photoanodes (ZnO NRs), including H. J. Tan (2021), resulting in a current density of up to 0.483 mA/cm^2 in a 0.1 M Na_2SO_3 liquid electrolyte [18]. In another study, a PEC system based on ZnO NRs/Au produced a current density of 30 A/cm^2 in 0.1 M Na_2SO_4 electrolyte [19]. Unfortunately, from these studies, they still use liquid electrolytes that cause the photoanode to corrode easily in a long enough duration, thus affecting the lifetime and performance of the PEC cell [20]. This problem is often encountered in PEC water splitting. When the semiconductor-based photoanode material is immersed in an electrolyte solution, the H$^+$ and OH$^-$ ions will continuously adsorb and desorb on the cell surface until they reach dynamic equilibrium [21]. This is the reason why corrosion can be easily found in photoanode materials. Previous research has tried to overcome corrosion by coating the ZnO Nr PEC cells using polyaniline/Au in 0.1 M Na_2SO_4 liquid electrolyte. However, the current density and efficiency of solar to hydrogen are still low, which are 10.6 μA/cm^2 and 0.16%, respectively (influence Au tommy 2020). Therefore, a solution is needed so that the ZnO Nr photoanode does not corrode easily. One solution proposed in this research is to use solid electrolytes instead of liquid electrolytes. The solid electrolyte used is Yttria Stabilized Zirconia (YSZ).

Yttria Stabilized Zirconia (YSZ) was chosen because it has high ionic conductivity (>1 × 10^{-3} S/cm) [22] and is chemically stable [23]. In previous research, the synthesis of Ni/YSZ for fuel cell electrochemical devices succeeded in obtaining an ionic conductivity of 2.25 × 10^{-4} S/cm and activation energy of 0.562 eV at a sintering temperature of 600 °C [24]. In another study, the MgO/YSZ for fuel cell electrochemical devices obtained a conductivity of 0.6 S/cm and activation energy of 0.45 eV at a sintering temperature of 800 °C [25]. However, research on PEC cells using solid electrolytes with sintering temperatures above 800 °C is still rare. Therefore, this study combines YSZ-based solid electrolytes with ZnO NRs films as photoanodes in PEC cells. The variation used is the sintering temperature of YSZ solid electrolyte (1000, 1200 and 1400 °C) coated with ZnO NRs film with a layered arrangement is expected to reduce corrosion and improve corrosion performance in PEC cell devices.

2. Research procedure

The ZnO nanorods were synthesized in two steps. The first stage was the manufacture of ZnO Seed Layer. Synthesis of ZnO solution occurs by mixing 0.88 g of Zinc Acetate Dihydrate and 0.24 L MEA in 20 mL of Ethanol pa using the sol gel method. First, the ZnO seed layer deposition is carried out on the ITO Glass substrate with the spin coating method at a speed of 3000 rpm for 30 s, then heated at 400 °C for 2 h. The second stage is the growth of nanorods using the hydrothermal method. The precursors used are 0.58 g of Zinc Nitrate Dehydrate and 0.32 g of hexamethylenetetramine (HMTA) with a growing temperature of 115 °C for 5 h. Finally, the ZnO NRs are annealed at 500 °C for 2 h. This film preparation is illustrated in Fig. 1.

The first thing to perform for the synthesis of YSZ solid electrolyte is the sintering of the YSZ powder at the temperatures of 1000, 1200 and 1400 °C, then dissolve it with 300 L IPA (Isopropyl Acohol) and 180 L HNO$_3$ to form a paste. It is then
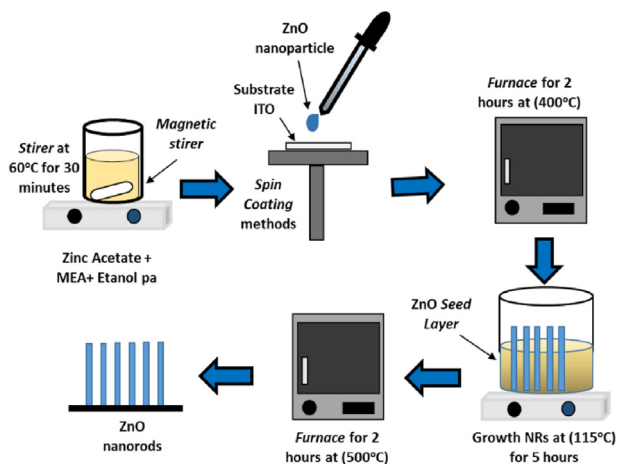
Fig. 1 − Preparation of ZnO seed layer and ZnO nanorods.

deposited on the ZnO film using the knife coating technique. Finally, the sample is annealed at 150 °C for 30 min as illustrated in Fig. 2.

The counter electrode used in this study is Activated Carbon. The sol gel method was used to synthesize Activated Carbon (AC). A total of 2 g of AC powder was mixed with 0.2 g of PVDF, then dissolved with 5 mL of NMP, and later stirred for 24 h at 600 rpm. Activated carbon paste was deposited using the knife coating technique on the Silicon wafer substrate. Then it was sintered at 100 °C for 10 min. The layer structure is shown in Fig. 3.

Then the ZnO NRs/YSZ samples were characterized by XRD, SEM-EDX, and UV−Vis. The efficiency of the PEC cell device is known from the I−V test on the solar simulator with PEC-CELL software. This test determines the maximum current efficiency produced by the film added with photodetector testing, such as current photoresponse.

3. Results and discussion

XRD analysis was performed to determine the crystallinity and characteristics of ZnO NRs and ZnO NRs/YSZ with
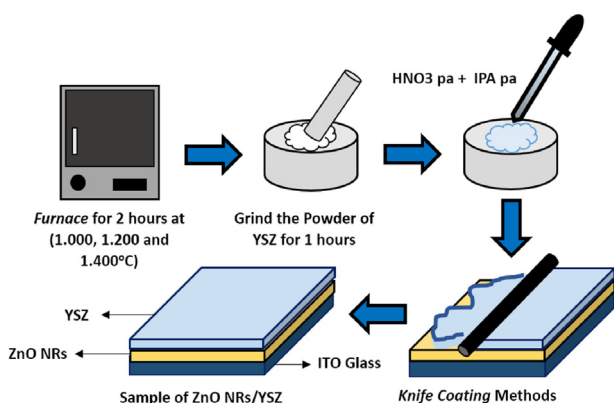
Fig. 2 − Preparation of YSZ. Solid electrolyte.
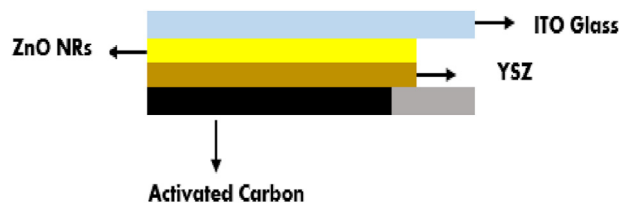
Fig. 3 − Arrangement of ZnO NRs/YSZ. Thin films.

different YSZ annealing treatments. Fig. 4(a) shows the ZnO NRs as a single phase with a hexagonal crystal structure of the Wurtzite phase, space group P6$_{3mc}$. The ZnO lattice parameters are a, b = 3.250 Å, and c = 5.205 Å [12] and they complied with (AMCSD) No. 005203 [26]. While YSZ has a cubic crystal structure with a space group Fm-3m [27] with YSZ lattice parameters are a, b, c = 5.154 Å [28]. Fig. 4(b), (c), and (d) are the results of the refinement of ZnO NRs/YSZ with variations in the YSZ activation temperature. The activation temperatures given are 1000, 1200 and 1400 °C, respectively.

Sample of ZnO NRs in Fig. 4(a) show the orientation of the characteristic peaks at 2θ; 31.7°, 34.4°, and 36.2° with crystal planes (010), (002), and (011) [29]. Meanwhile, the ZnO NRs/YSZ samples show the dominant orientation of ZnO characteristics at position 2θ; 34.8° with the crystal plane (002) and the YSZ peak at position 2θ; 30.1°, 50.3° and 59.9° with crystal planes (111), (220) and (311). In position 2θ, the diffraction pattern is in accordance with the research conducted by Ravi Aggarwal et al. [30]. When the nucleation rate is faster, the growth of particles with a less agglomeration is obtained, and the formation of a perfect hexagonal rod structure is lower [31]. In addition, the higher annealing temperature at YSZ increases the inter-electrostatic potential and shows a higher tendency to form larger particle sizes in accordance with the Scherrer equation (Equation (1)). The particles size based on the equation are 124, 129 and 134 nm along with the increasing activated temperature.
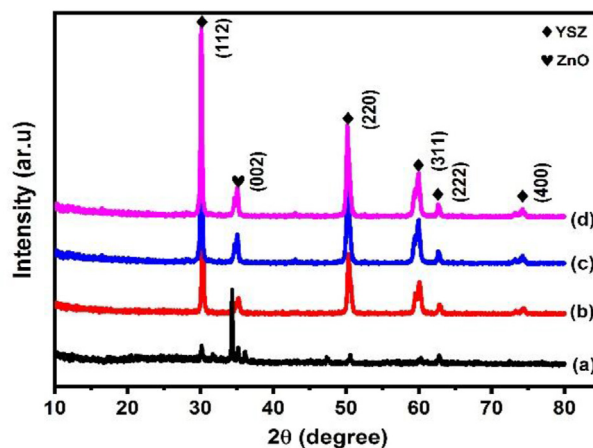
Fig. 4 − Diffraction pattern (a) ZnO NRs, ZnO NRs/YSZ at several activation temperatures YSZ (b) 1000, (c) 1200 and (d) 1400 °C.
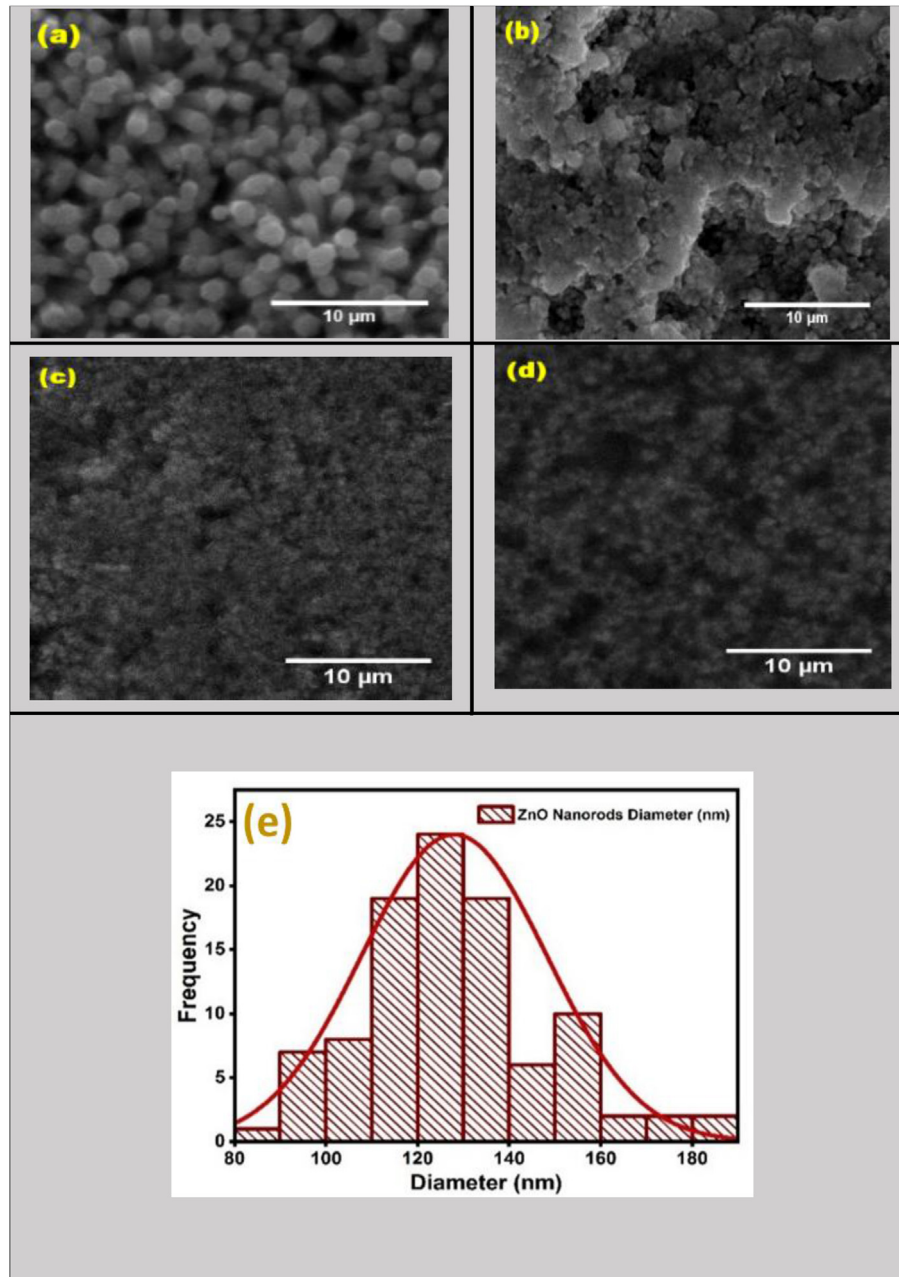
Fig. 5 — Top view SEM (a) ZnO NRs, and ZnO NRs/YSZ sintered at temperatures (b) 1000, (c) 1200, (d) 1400 °C, and (e) particle size distribution of YSZ.

$$\tau = \frac{K\lambda}{\beta \cos \theta} \tag{1}$$

SEM testing was carried out with a magnification of 50,000 times to characterize the surface morphology of the ZnO NRs and ZnO NRs/YSZ samples with variation of YSZ activation temperature. The test results are shown in Fig. 5(a)—(d). In the top view of the ZnO NRs sample, it can be observed that the rods manage to form a hexagonal, which is consistent with the XRD results. The diameters of ZnO NRs were measured and plotted using ImageJ and Origin software, respectively.

The analysis results indicate the average rod value of 125 nm, as seen by the distribution curve plot in Fig. 5(e). The average diameter of this rod is in accordance with previous research conducted by Tyona et al. [32].

In the top view of the ZnO NRs/YSZ samples with YSZ activation temperature variations, the surfaces of all the samples are agglomerated, as shown in Fig. 5(b)—(d). This agglomeration is a characteristic of the YSZ ceramics materials. It is found that the higher applied activation temperature, the lower agglomeration rate became. This is due to the
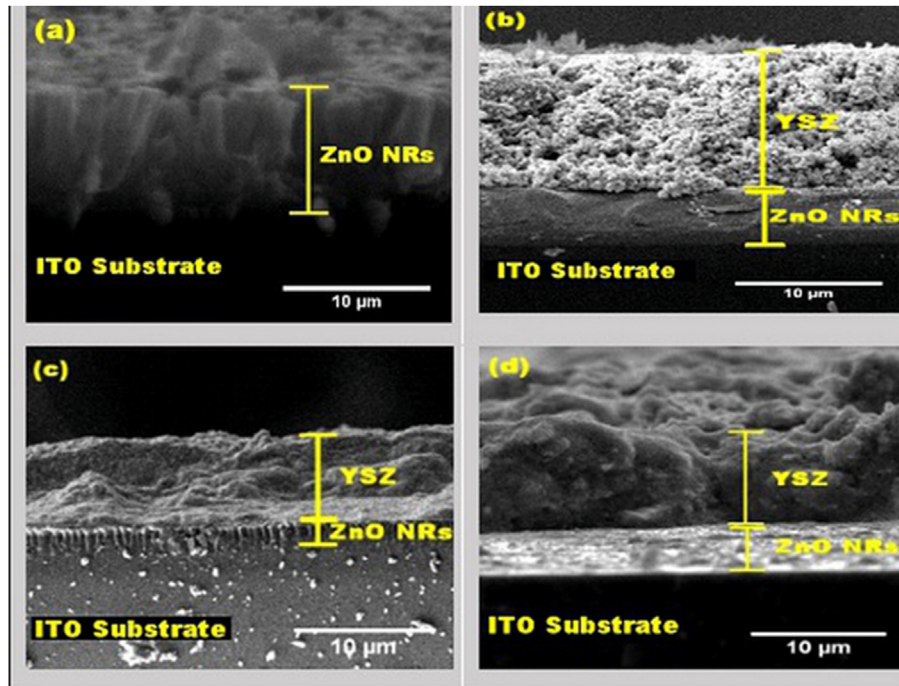
Fig. 6 – Cross section of ZnO NRs and ZnO NRs/YSZ with variations in temperature. Activation of solid electrolyte (a) ZnO NRs, (b) ZnO NRs/YSZ 1000 °C, (c) ZnO NRs/YSZ 1200 °C, (d) ZnO NRs/YSZ 1400 °C, and (e) trend of sample thickness which shows a decrease with increasing activation temperature.
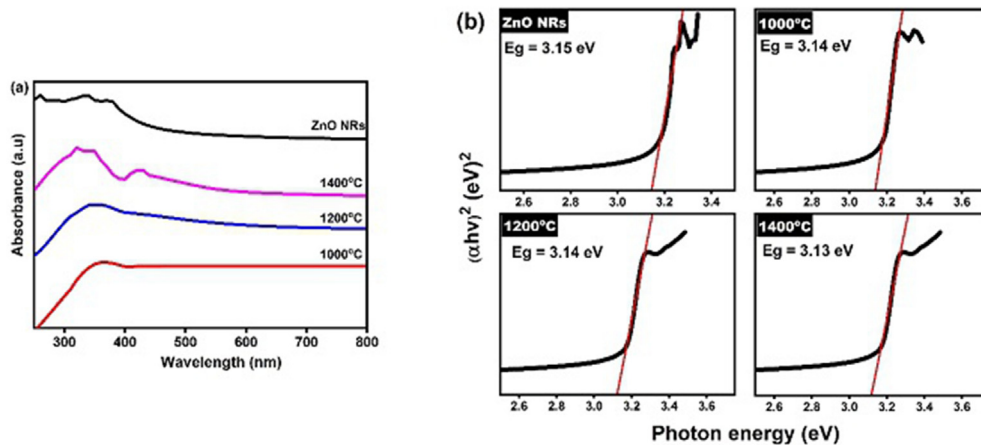
Fig. 7 – (a) Absorbance graph and (b) band gap of ZnO NRs and ZnO NRs/YSZ at several YSZ activation temperatures.

activation temperature of YSZ, which is above 1250 °C with detention for 2 h, making the YSZ material which originally formed coarse (becomes denser) with a low agglomeration rate [33]. In accordance with the results of the XRD analysis, which show the increasing of particle size, the denser YSZ causes more voids in the YSZ to be filled. This causes the YSZ to become denser and thinner, as shown in Fig. 6.

Based on the results of the SEM cross section, it is observed that the YSZ layer is clearly visible Fig. 6. The thickness of the thin film is influenced by several things. The

Table 1 – Absorbance wavelength and band gap ZnO NRs/YSZ.		
Sample	Absorbance (nm)	Band gap (eV)
ZnO nanorods	380	3.15
ZnO NRs/YSZ (1000 °C)	385	3.14
ZnO NRs/YSZ (1200 °C)	392	3.14
ZnO NRs/YSZ (1400 °C)	422	3.13
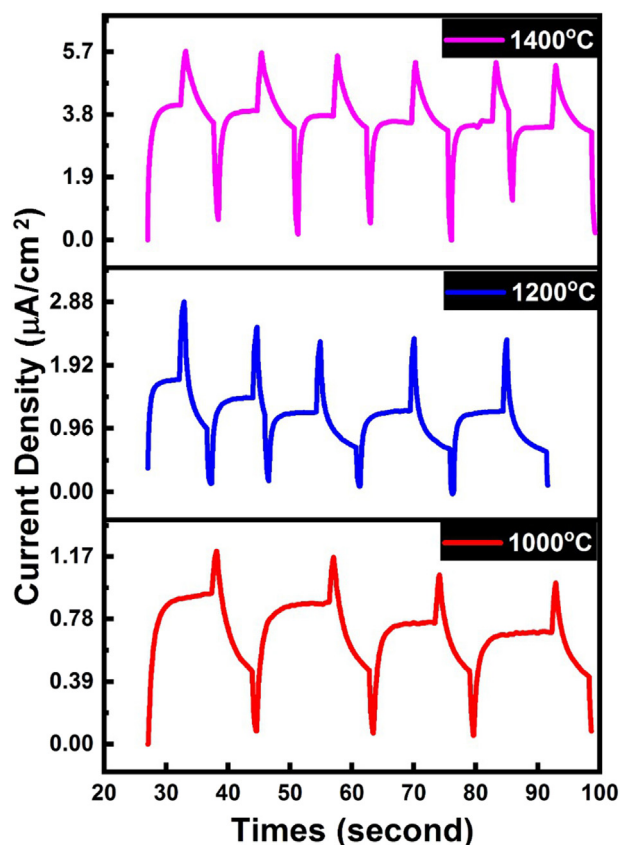
Fig. 8 – Photoresponse of ZnO NRs/YSZ.

thickness of the ZnO seed layer can be affected during the spin coating process. Both the rpm speed and the amount of ZnO solution that is dropped. The tendency of the YSZ layer to thin out is caused by the decreasing level of YSZ agglomeration at high heating temperatures, as shown in Fig. 5. This decrease in agglomeration makes the knife coating deposition smoother. More particles fill the pores, so the layer becomes denser and thinner. Meanwhile, when the YSZ with high agglomeration is deposited, large agglomerate particles will be harder to fill in the pores so that more agglomerates will accumulate, resulting in a thicker YSZ layer.

Furthermore, Fig. 7(a) is a graph of the UV–Vis absorbance data processing, which shows the light absorption properties of ZnO NRs/YSZ measured in the wavelength range from 250 nm to 800 nm. The ZnO NRs samples and all the ZnO NRs/YSZ samples show an absorption edge at a wavelength of about 380 nm. It is accordance with the research conducted by Zhang et al. [19]. Based on the frequency spectrum of light, the absorbance wavelength range of this film is 380–422 nm. This shows that the film is able to absorb visible light wavelength range [18]. The absorbance value of ZnO NRs/YSZ samples increases with increasing activation temperature. This is due to the denser and thinner layer of YSZ leads to more absorbed light intensity.

Fig. 7(b) shows the band gap of ZnO NRs and ZnO NRs/YSZ with various activation temperatures. The graph shows that the higher the activation temperature of Yttria Stabilized Zirconia (YSZ), the smaller band gap appeared. This is because there is an oxygen vacancy in YSZ. This oxygen vacancy increases the electron potential that is localized to the vacancy site [34]. As a result, these localized electrons form donor levels close to the Fermi energy, so the band gap will decrease as the activation temperature increases.

In addition, the band gap value affects photon absorption in thin films, where the smaller the band gap, the more optical absorption occurs. This facilitates the transfer of electrons from the valence band to the conduction band [35]. The absorbance and band gap values are illustrated in Table 1.

Based on the analysis, it is known that the highest absorbance occurs in the material with the smallest band gap energy. Thus, it is concluded that this material is considerably good if applied as a solar cell device. Fig. 8 shows the photoresponse graph of the ZnO NRs/YSZ thin film at several YSZ activation temperatures. Testing this sample requires a solar simulator with a light source intensity of 100 mW/cm². From the graph, it is known that this thin film has a fairly good response.

It is shown that when the sample is illuminated by the solar simulator, the photocurrent shows a rapid increase followed by a slow increase without reaching saturation [36]. The sharp peak current occurs because of the synchronization process when there is a change from dark to light and vice versa [37]. In the absence of light, the photocurrent decreases continuously, then decreases slowly until it reaches a minimum value.

Fig. 10 is a photoresponse fitting of the current ZnO NRs/YSZ film. The graph between the current and time in light irradiation on or off can be matched using the exponential shown in Equation (2).

$$I = I_0 + A \exp(-t/\tau) \tag{2}$$

where I is the current as a function of time, A is the amplitude, t is the time, τ is the relaxation time constant. This will determine the ride time (τ_r) and decay time (τ_d).

The graph shows that the rising response time of ZnO NRs/YSZ is shorter than the decay time shown in Fig. 9. This is because the light hitting the ZnO NRs/YSZ film produces electron–hole pairs. Thus, it is easier for electrons to be excited from the valence band to the conduction band. At the same time, the holes will oxidize the oxygen ions on the surface. When there is no light, the reaction with oxygen ions is difficult to release because the oxidation process takes a long time [38].

From the photoresponse graph of the current measurement, it is found that the higher the activation temperature when irradiated, the faster the response time of ZnO NRs/YSZ. However, as evidenced by the sample, response time is still less than 1 s. Meanwhile, even though the response is not linearly faster when dark, the time required is still less than
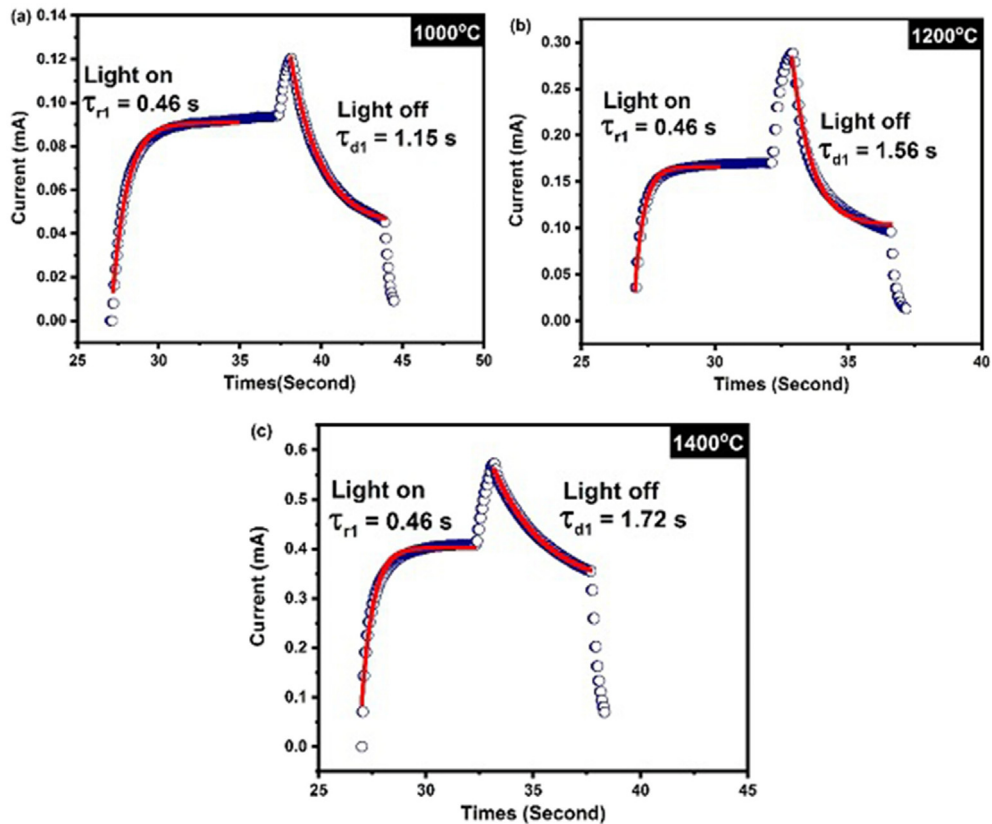
Fig. 9 – Photoresponse fitting current ZnO NRs/YSZ at several activation temperatures YSZ.

2 s. This is because as the activation temperature of YSZ increases, the ionic conductivity also increases.

Ion conductivity itself is the movement of ions due to the presence of electricity. Therefore, the movement of ions in the ZnO NRs/YSZ samples during testing becomes faster, which shortens the relaxation time as the activation temperature increases. The results of photoresponse fittings are shown in Table 2. The I–V testing of the ZnO NRs/YSZ films was accomplished using a solar simulator and PEC-CELL software. Based on the graph, Equations (3) and (4) are obtained to determine the efficiency of the PEC cells [39].

$$FF = \frac{V_{max} \times I_{max}}{V_{oc} \times I_{sc}} \qquad (3)$$

$$\eta = \frac{V_{oc} \times I_{sc} \times FF}{100} \times 100\% \qquad (4)$$

Based on the results of the analysis that have been carried out, the current efficiency of the ZnO NRs/YSZ samples at the

temperatures of 1000, 1200 and 1400 °C is 0.64, 0.70 and 1.00%, respectively. The graph of the efficiency of ZnO NRs/YSZ thin films at several YSZ activation temperatures is shown in Fig. 10.

It can be concluded that the higher the YSZ activation temperature, the higher the efficiency of the current generated. This is in accordance with the research conducted by Guan et al., where the optimum YSZ activation temperature was produced above 927 °C. This happens because, at high temperatures, oxygen anions in YSZ are no longer retained in the lattice. This causes delocalization, resulting in oxygen vacancy gradually occurring in the hkl plane (112) [40]. The parameters of the results of the ZnO NRs/YSZ sample fittings are shown in Table 3.

4. Conclusion

The increase in the YSZ activation temperature on the ZnO NRs/YSZ thin films causes the crystallinity of ZnO NRs/YSZ to be higher. The highest agglomeration occurs in the sample with the lowest activation temperature. The increase in the YSZ activation temperature also causes oxygen vacancy in the YSZ solid electrolyte, causing the band gap to become smaller. This is inversely proportional to the absorbance value of this thin film wavelength. This is because the highest optical absorption occurs in the sample with the highest crystallinity. In the Photodetector test, it is found that the

Table 2 – Photoresponse current fittings ZnO NRs/YSZ.		
Sample ZnO NRs/YSZ	Light on (τ_{r1}) (s)	Light off (τ_{d1}) (s)
1000 °C	0.74	1.15
1200 °C	0.72	1.56
1400 °C	0.46	1.72
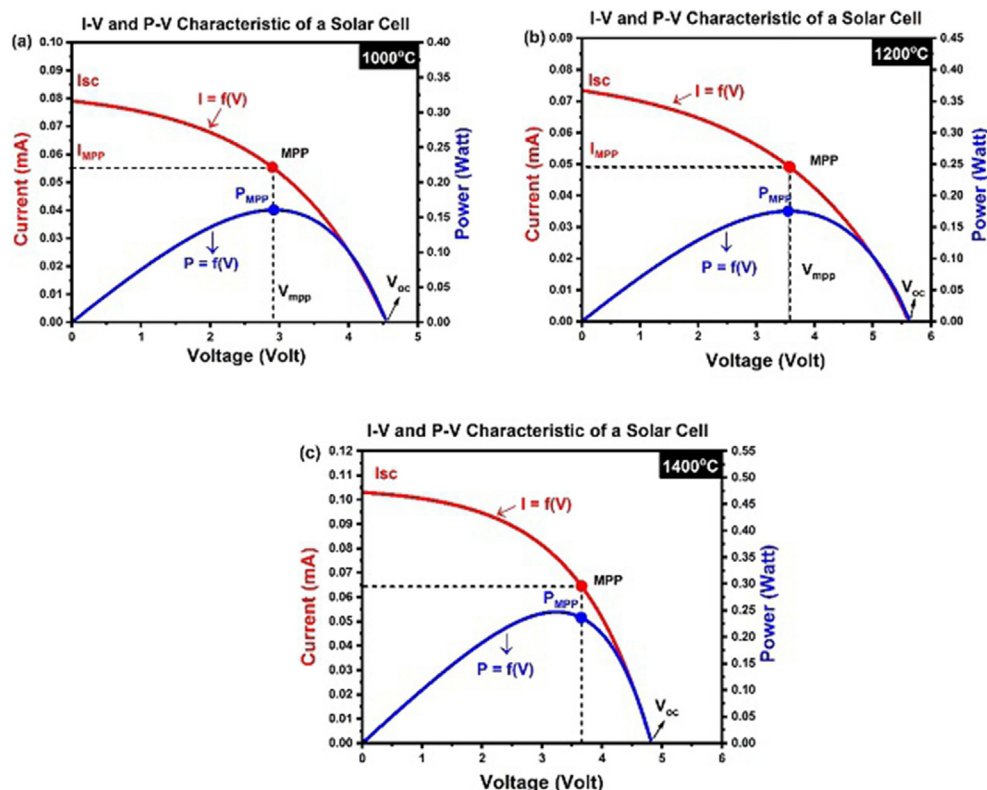
Fig. 10 — Graph of ZnO/YSZ efficiency.

Table 3 — Efficiency parameters of PEC ZnO NRs/YSZ cells.

Parameter	1000 °C	1200 °C	1400 °C
R_s (ohm)	10.12	14.27	10.03
I_{sc} (mA)	0.25	0.22	0.32
J_{sc} (mA/cm^2)	0.50	0.44	0.64
V_{oc} (V)	2.53	3.14	3.21
Fill factor	0.39	0.39	0.50
P_{max} (W)	1.61	1.76	2.07
I_{max} (mA)	0.35	0.32	0.43
V_{max} (V)	4.60	5.49	4.83
Efficiency (%)	0.64	0.70	1.00

higher the activation temperature, the faster the response of the sample. This owes to the higher conductivity of the ions produced. Finally, the highest efficiency of the photo-electrochemical cell device is found in the sample with an activation temperature of 1400 °C, which is 1%. This happens because, at high temperatures, oxygen anions in YSZ are no longer retained in the lattice and cause delocalization, resulting in gradually oxygen vacancy.

Declaration of Competing Interest

The authors declare that they have no known competing financial interests or personal relationships that could have appeared to influence the work reported in this paper.

REFERENCES

[1] Gençer E, Agrawal R. A commentary on the US policies for efficient large scale renewable energy storage systems: focus on carbon storage cycles. Energy Pol 2016;88:477—84. https://doi.org/10.1016/j.enpol.2015.11.003.

[2] Arshad M, Ahmed S. Cogeneration through bagasse: a renewable strategy to meet the future energy needs. Renew Sustain Energy Rev 2016;54:732—7. https://doi.org/10.1016/j.rser.2015.10.145.

[3] Green MA. Erratum: solar cell efficiency tables (version 46) (Progress in Photovoltaics: Research and Applications (2015) 23 (805—812)). Prog Photovolt Res Appl 2015;23(9):1202. https://doi.org/10.1002/pip.2667.

[4] Finegold L, Cude JL. Biological sciences: one and two-dimensional structure of alpha-helix and beta-sheet forms of poly(L-alanine) shown by specific heat measurements at low temperatures (1.5—20 K). Nature 1972;238(5358):38—40. https://doi.org/10.1038/238038a0.

[5] Of T, For E. Fixation strength of a new device for soft tissue anterior. arXiv:1706.01493 [cond-mat.mtrl-sci] 2017.

[6] Passalacqua R, Perathoner S, Centi G. Semiconductor, molecular and hybrid systems for photoelectrochemical solar fuel production. J Energy Chem 2017;26(2):219—40. https://doi.org/10.1016/j.jechem.2017.03.004.

[7] Jiang C, Moniz SJA, Wang A, Zhang T, Tang J. Photoelectrochemical devices for solar water splitting-materials and challenges. Chem Soc Rev 2017;46(15):4645—60. https://doi.org/10.1039/c6cs00306k.

[8] Bai Z, Yan X, Kang Z, Hu Y, Zhang X, Zhang Y. Photoelectrochemical performance enhancement of ZnO photoanodes from ZnIn2S4 nanosheets coating. Nano Energy 2015;14:392—400. https://doi.org/10.1016/j.nanoen.2014.09.005.

[9] Klingshirn C. ZnO: material, physics and applications. ChemPhysChem Apr. 2007;8(6):782—803. https://doi.org/10.1002/cphc.200700002.

[10] Chen C, Bai Hongye, Da Zulin, Li Meng, Yan Xu, Jiang Jinhui, et al. Hydrothermal synthesis of Fe_2O_3/ZnO heterojunction photoanode for photoelectrochemical water splitting. Funct Mater Lett 2015;8(5):10—3. https://doi.org/10.1142/S1793604715500587.

[11] Ong CB, Ng LY, Mohammad AW. A review of ZnO nanoparticles as solar photocatalysts: synthesis, mechanisms and applications. Renew Sustain Energy Rev 2018;81:536—51.

[12] Mufti N, Hasan Abadi M Tommy, Yasrina Atsnaita, Sunaryono Sunaryono, Yudyanto Yudyanto, Diantoro Markus, et al. Photoelectrochemical performance of ZnO nanorods grown on stainless steel substrate. IOP Conf Ser Mater Sci Eng 2019;515(1). https://doi.org/10.1088/1757-899X/515/1/012023.

[13] Zhu L, Zeng W. Room-temperature gas sensing of ZnO-based gas sensor: a review. Sensor Actuator Phys 2017;267:242—61.

[14] Purushothaman KK, Priya VS, Nagamuthu S, Vijayakumar S, Muralidharan G. Synthesising of ZnO nanopetals for supercapacitor applications. Micro Nano Lett Aug. 2011;6(8):668—70. https://doi.org/10.1049/mnl.2011.0260.

[15] Mufti N, Maryam S, Fibriyanti AA, Kurniawan R, Fuad A, Taufiq A. Morphological modification and analysis of ZnO nanorods and their optical properties and polarization. Scanning 2018;2018.

[16] Mehrabian M, Aslyousefzadeh S, Maleki MH. Highly efficient hybrid solar cell using ZnO nanorods and assessment of changes in cell performance by varying the growth period. J Korean Phys Soc 2015;66(10):1527—31.

[17] Song J, Lim S. Effect of seed layer on the growth of ZnO nanorods. J Phys Chem C Jan. 2007;111(2):596—600. https://doi.org/10.1021/jp0655017.

[18] Tan HJ, Zainal Zulkrnain, Talib ZA, Lim HN, Shafie Suhaidi, Tan ST, et al. Synthesis of high quality hydrothermally grown ZnO nanorods for photoelectrochemical cell electrode. Ceram Int 2021;47(10):14194—207. https://doi.org/10.1016/j.ceramint.2021.02.005.

[19] Zhang W, Wang W, Shi H, Liang Y, Fu J, Zhu M. Surface plasmon-driven photoelectrochemical water splitting of aligned ZnO nanorod arrays decorated with loading-controllable Au nanoparticles. Sol Energy Mater Sol Cell 2018;180(November 2017):25—33. https://doi.org/10.1016/j.solmat.2018.02.020.

[20] Chang CY, Huang YC, Tsao CS, Su WF. Formation mechanism and control of perovskite films from solution to crystalline phase studied by in situ synchrotron scattering. ACS Appl Mater Interfaces 2016;8(40):26712—21. https://doi.org/10.1021/acsami.6b07468.

[21] van de Krol R. Principles of photoelectrochemical cells. In: van de Krol R, Grätzel M, editors. Photoelectrochemical hydrogen production. Boston, MA: Springer US; 2012. p. 13—67. https://doi.org/10.1007/978-1-4614-1380-6_2.

[22] Brett DJL, Atkinson A, Brandon NP, Skinner SJ. Intermediate temperature solid oxide fuel cells. Chem Soc Rev 2008;37(8):1568—78. https://doi.org/10.1039/b612060c.

[23] Ivers-Tiffée E, Weber A, Herbstritt D. Materials and technologies for SOFC-components. J Eur Ceram Soc 2001;21(10—11):1805—11. https://doi.org/10.1016/S0955-2219(01)00120-0.

[24] Esposito V, Gadea C, Hjelm J, Marani Debora, Hu Qiang, Agersted K, et al. Fabrication of thin Yttria-Stabilized-Zirconia dense electrolyte layers by inkjet printing for high performing solid oxide fuel cells. J Power Sources Jan. 2015;273:89—95. https://doi.org/10.1016/j.jpowsour.2014.09.085.

[25] Kosacki I, Rouleau CM, Becher PF, Bentley J, Lowndes DH. Surface/interface-related conductivity in nanometer thick YSZ films. Electrochem Solid State Lett 2004;7(12):459—61. https://doi.org/10.1149/1.1809556.

[26] Poornaprakash B, Chalapathi U, Subramanyam K, Vattikuti SVP, Park SH. Wurtzite phase Co-doped ZnO nanorods: morphological, structural, optical, magnetic, and enhanced photocatalytic characteristics. Ceram Int 2020;46(3):2931—9. https://doi.org/10.1016/j.ceramint.2019.09.289.

[27] Ishizawa N, Matsushima Y, Hayashi M, Ueki M. Synchrotron radiation study of yttria-stabilized zirconia, Zr0.758Y0.242O1.879. Acta Crystallogr Sect B Struct Sci 1999;55(5):726—35. https://doi.org/10.1107/S0108768199005108.

[28] Wang H, Dinwiddie RB, Porter WD. Development of a thermal transport database for air plasma sprayed ZrO2-Y2O3 thermal barrier coatings. J Therm Spray Technol 2010;19(5):879—83. https://doi.org/10.1007/s11666-010-9486-z.

[29] Ahmed F, Kumar S, Arshi N, Anwar MS, Prakash R. Growth and characterization of ZnO nanorods by microwave-assisted route: green chemistry approach. Adv Mater Lett 2011;2(3):183—7. https://doi.org/10.5185/amlett.2011.1213.

[30] Aggarwal R, Zhou H, Jin C, Narayan J, Narayan RJ. Semipolar r-plane ZnO films on Si(100) substrates: thin film epitaxy and optical properties. J Appl Phys 2010;107(11). https://doi.org/10.1063/1.3406260.

[31] Ridhuan NS, Abdul Razak K, Lockman Z, Abdul Aziz A. Structural and morphology of ZnO nanorods synthesized using ZnO seeded growth hydrothermal method and its properties as UV sensing. PLoS One 2012;7(11):e50405.

[32] Tyona MD. Doped zinc oxide nanostructures for photovoltaic solar cells application. Zinc oxide based nano materials and devices. 2019. p. 1—18. https://doi.org/10.5772/intechopen.86254.

[33] Patil DS, Prabhakaran K, Dayal Rajiv, Prasad Durga, Gokhale NM, Samui AB, et al. Eight mole percent yttria stabilized zirconia powders by organic precursor route. Ceram Int 2008;34(5):1195—9. https://doi.org/10.1016/j.ceramint.2007.02.013.

[34] Li G, Blake GR, Palstra TTM. Vacancies in functional materials for clean energy storage and harvesting: the perfect imperfection. Chem Soc Rev 2017;46(6):1693—1706, Mar. https://doi.org/10.1039/C6CS00571C.

[35] Zhu W, Xiao H. First-principles band gap criterion for impact sensitivity of energetic crystals: a review. Struct Chem 2010;21(3):657—65. https://doi.org/10.1007/s11224-010-9596-8.

[36] Keem K, Kim H, Tae Kim G, Lee JS, Min B, Cho K, et al. Photocurrent in ZnO nanowires grown from Au electrodes. Appl Phys Lett 2004;84(22):4376—8. https://doi.org/10.1063/1.1756205.

[37] Zhang Y, Hellebusch DJ, Bronstein ND, Ko C, Olgletree DF, Salmeron M, et al. Ultrasensitive photodetectors exploiting electrostatic trapping and percolation transport. Nat Commun 2016;7(May):1—9. https://doi.org/10.1038/ncomms11924.

[38] Dai W, Pan X, Chen S, Wen Z, Zhang H, Ye Zhizhen. Honeycomb-like NiO/ZnO heterostructured nanorods: photochemical synthesis, characterization, and enhanced UV detection performance. J Mater Chem C 2014;2(23):4606—14. https://doi.org/10.1039/c4tc00157e.

[39] Priambodo PS, Poespawati NR, Hartanto D. Solar cell. no. November. 2011. https://doi.org/10.5772/19935.

[40] Guan SH, Shang C, Liu ZP. Resolving the temperature and composition dependence of ion conductivity for yttria-stabilized zirconia from machine learning simulation. J Phys Chem C 2020;124(28):15085—93. https://doi.org/10.1021/acs.jpcc.0c04331.